Control of spatiotemporal rogue waves by harmonic pump modulation in a semiconductor laser with a saturable absorber

Control of spatiotemporal rogue waves by harmonic pump modulation in a semiconductor laser with a saturable absorber

K. Talouneh,[1] C. Rimoldi,[2] R. Kheradmand,[3,1] G. Tissoni,[4] and M. Eslami[5,*]
[1]*Research Institute for Applied Physics and Astronomy, University of Tabriz, Tabriz, Iran*
[2]*INRS-EMT, 1650 Boulevard Lionel-Boulet, Varennes, Québec, Canada J3X 1S2*
[3]*Faculty of Physics, University of Tabriz, Tabriz, Iran*
[4]*Université Côte dAzur, CNRS, Institut de Physique de Nice, Valbonne, France*
[5]*Department of Physics, University of Guilan, P.O. Box 41335-1914, Rasht, Iran*

(Received 13 May 2020; accepted 14 August 2020; published 10 September 2020)

Through numerical simulations, statistical and dynamical properties of extreme events in a broad-area semiconductor laser with intracavity saturable absorber are investigated. By inclusion of a diffusion coefficient for the field, formation of rogue waves in a state of extended turbulence is studied and shown to be affected by harmonic perturbations. In particular, we propose a control technique based on periodic modulation of the pump parameter which can either drive the state of the system closer to or away from the chaotic attractors respectively enhancing or suppressing the generation of rogue waves. By statistical and dynamical analysis of the events in terms of intensity and optical gain, we show that when the system is under resonant modulation with frequency close to that of the dominant oscillations in the turbulent state (which is equal to the relaxation oscillation frequency typical of semiconductor lasers), more rogue waves are triggered with larger intensities and shorter lifetimes. On the other hand, off-resonant modulations restrain the formation of rogue waves where they appear in lower intensities and longer lifetimes. An example of special cases where the proposed scheme can completely forbid or allow the emission of rogue waves is also presented.

DOI: 10.1103/PhysRevA.102.033508

I. INTRODUCTION

Extreme events, long thought of as high-impact, unpredictable, and clueless incidents, occur in systems of natural, technical, and societal settings. They are almost a necessary manifestation of a complex dynamics inherent in such systems. In the form of waves, they are referred to as rogue waves (RWs) and were first observed and studied in oceanography and hydrodynamics. After an analogy was found between the generation of large ocean waves and the propagation of light fields in optical fibers, researchers in optics and photonics became interested in investigation of optical RWs. The surging interest dates back to the seminal paper of Solli *et al.* [1], where extraordinary high-amplitude peaks were observed in supercontinuum generation in optical fibers. Over the course of more than 10 years, many optical systems have been studied for RWs, their generating mechanisms, and their characterization. They include solitons in integrable systems [2–5] and their dissipative counterparts [6,7], spatiotemporal chaos [8,9], coexistent disorder and nonlinearity [10,11], or modulational instability [12,13]. Such studies have also been extended to mechanisms where the dimensionality matters, for example, complexity arising from low-dimensional chaos [14,15], many longitudinal modes in a one-dimensional system [16–20], and spatially extended in the transverse dimensions where spatial coupling occurs via diffraction [21,22].

While there can be found various subjective definitions for RWs (as with being rare, destructive, etc.) [23], researchers in nonlinear optical systems have narrowed it down to objective definitions regardless of the underlying generating mechanism and environment-dependent considerations [24]. All these definitions share the same basis that the pulses should be of high enough amplitude compared to the more frequently occurring pulses in the same environment. However, when it comes to the minimum height of those pulses to be characterized as rogue, people have used different criteria. On the other hand, for the purpose of characterization researchers still have to focus on the dynamical and statistical behavior of those events since the exact and adequate knowledge of them is unavailable. Moreover, their control, management, and prediction have recently become of significant importance and already drawn the attention of many researchers [15,25–29]. For example, in [25,26] external forcing is used to control the likelihood of RW emission in an injected semiconductor laser which is enabled by the modulation phase. Occurrence of these phenomena naturally depends on the quality, accuracy, and availability of data, existence and type of precursors, and the amount of determinism involved in the dynamics which make prediction a challenging task (at least for a large time window). This is while rogue wave control and management can be extremely useful requiring a deep understanding of the underlying mechanisms.

Broad-area semiconductor lasers with intracavity saturable absorber, two-dimensional systems in nature, have recently been investigated numerically and experimentally for extreme events [7,30], where extended turbulence and chaos prepare

*Corresponding author: meslami@guilan.ac.ir

the formation of RWs. We should note that the experiments in [30] are 1D because they eliminate one of the directions by using a linear pump and the rest of the device is not pumped. Here, we instead focus on the control of RWs' occurrences in the same model and propose a control technique based on harmonic modulation of the input pump current. We show, by numerical simulations of the broad-area semiconductor laser containing saturable absorber, that multiple solutions are present below laser threshold including stationary, chaotic, and self-pulsing cavity solitons (CSs) along with a high-intensity turbulent branch which remains the only stable solution beyond the laser threshold. It is particularly shown that when the system is excited by harmonic modulation close to the undamped relaxation oscillation frequency, statistics and dynamics of the events change and the state of the system exhibits RWs more in number, higher in intensity, and fast in time duration. Resonant excitation has already been shown to be an effective tool to achieve an ultralow energy switch in the same system due to the very efficient excitation of Goldstone modes close to the drift instability threshold [31]. On the other hand, we show that when the pump current is modulated far from resonance (with a frequency larger than the dominant undamped relaxation oscillations), RWs appear in fewer numbers, lower intensities, and longer duration. We support our claim by statistical analysis of the events and intensity-optical gain dynamics. All our numerical simulations and statistical analyses are in 2D.

These findings are unlike those reported in [26] where, for an optically injected semiconductor laser lacking spatial dynamics and the diffusion coefficient described by a set of rate equations, RWs have been shown to be fully suppressed for modulation frequencies near the relaxation oscillation frequency. The importance of frequency in such control methods based on periodic modulations has also been discussed in a spatiotemporal system where multistability (as the dominant feature) is due to the coupling of nonlinearity and diffraction [32]. In that system, the resonant interaction of the control frequency with the frequency of damped oscillations of the associated attractor can result in the annihilation of one or the other attractors, thus providing the operator with the choice of the final state from different multistable solutions.

The paper is organized in the following order: in Sec. II the model equations and stationary or dynamical solutions are presented, Sec. III is devoted to the discussions on the extended turbulent solutions and the statistical description of the events which form in such a state, periodic modulation of the pump and its effect on the statistics and properties of the RWs are included in Sec. IV, followed by the final remarks in the Conclusion section.

II. MODEL

An effective model describing a broad-area semiconductor laser containing saturable absorber, schematically shown in Fig. 1, is given by the following set of equations for intracavity field and populations in the two media (absorber and amplifier) [7]:

$$\begin{aligned}\partial_t F &= [(1-i\alpha)D + (1-i\beta)d - 1 + (\delta+i)\nabla^2]F,\\ \partial_t D &= b[\mu - D(1+|F|^2) - BD^2],\\ \partial_t d &= rb[-\gamma - d(1+s|F|^2) - Bd^2],\end{aligned} \tag{1}$$

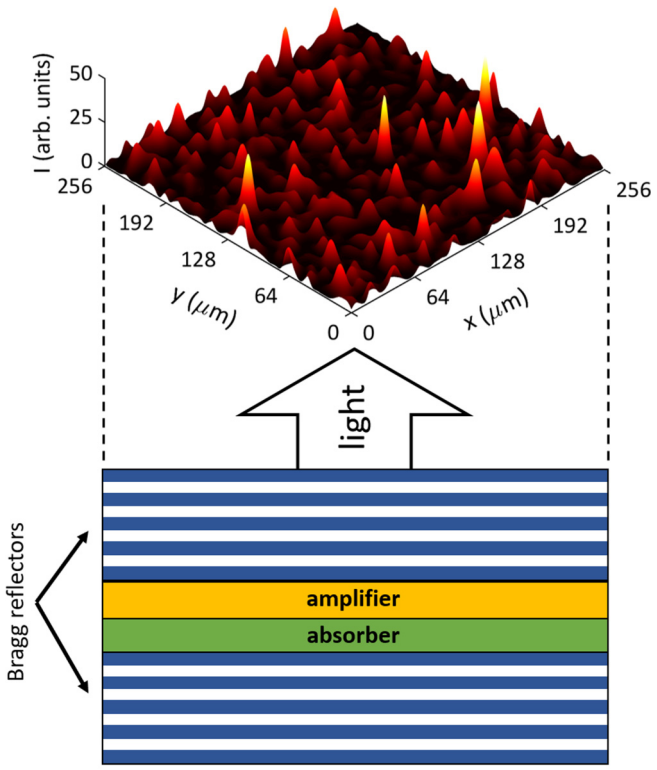

FIG. 1. Schematic representation of a broad-area semiconductor laser containing saturable absorber. An electric current modulator can be used for pump current modulation which is applied on the amplifier region.

where F is the slowly varying amplitude of the electric field and D, d are the population variables defined as

$$D = \eta_1(N_1/N_{1,0} - 1), \quad d = \eta_2(N_2/N_{2,0} - 1). \tag{2}$$

In Eq. (2), N_1 and N_2 are the carrier densities in the active and passive materials, respectively; $N_{1,0}$ and $N_{2,0}$ are their transparency values and η_1, η_2 are dimensionless coefficients related to gain and absorption, respectively. δ is a diffusion coefficient for the electric field that sets a filter to the number of spatial frequencies involved in the dynamics. Although it has been introduced phenomenologically making the present model different from that used in [33,34], a detailed derivation can be found in [35,36] and comes from the fact that a diffusion term in the electric field equation is needed to avoid structural instability of the equations. The parameters α (β) and b are the linewidth enhancement factor in the active (passive) material and the ratio of the photon lifetime to the carrier lifetime in the active material. The ratio of the carrier lifetime in the amplifier to that in the absorber is denoted by r. μ is the pump parameter of the active material, γ is the absorption parameter of the passive material, s is the saturation parameter, and B is the coefficient of radiative recombination. Time is scaled to the photon lifetime and space to the diffraction length. Typically, a time unit is a few ps and a space unit $\sim$4 μm. The integration of the dynamical equations is done by a split-step method separating the time and space derivatives on a 256 $\times$ 256 spatial grid, with space step 0.25 implying the physical distance of 1 μm between

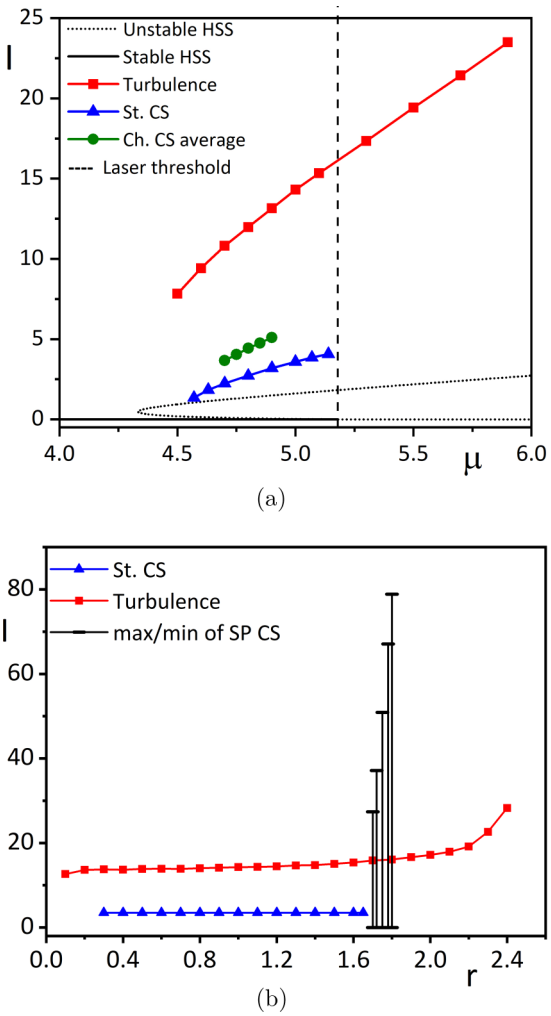

FIG. 2. Different solutions simultaneously present for (a) fixed $r = 1$ and varying μ and (b) fixed $\mu = 5$ and varying r. St., Ch., and SP respectively stand for stationary, chaotic, and self-pulsing. Note that parameter values of existence for self-pulsing CSs are $\mu =$ 4.7–5.12 and $r = 1.57$–1.82; thus they do not appear in (a).

two consecutive grid points. It uses the fast Fourier transform (FFT) for the Laplacian and Runge-Kutta for time derivatives along with the periodic boundary condition. We have used the following parameter values throughout the paper unless stated otherwise: $\delta = 0.01$, $s = 1$, $B = 0.1$, $\alpha = 2$, $\beta = 1$, $b =$ 0.01, and $\gamma = 2$. An important bifurcation parameter which is responsible for instabilities and is used here along with μ as the control parameter is r.

The model with $\delta = 0$ has already been shown to support localized and extended structures of various spatiotemporal dynamics including stationary, drifting, binary, self-pulsing, turbulent, and chaotic states [37–41]. However, to have a correct understanding of the extended turbulent states one needs to retain the diffusive term for the electric field, thus avoiding any unrealistic formation of filaments as a result of rapidly contracting spatial structures. Taking into account the diffusion coefficient for the field, the available solutions in the parameter space made up of intensity and a control parameter μ and r are shown respectively in Figs. 2(a) and 2(b).

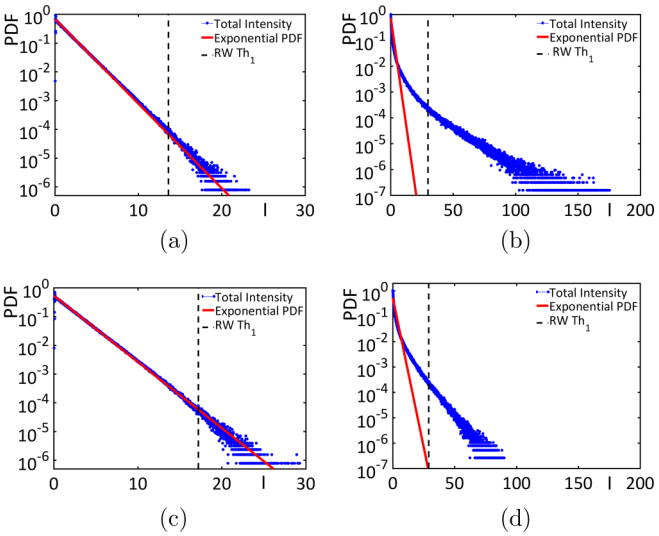

FIG. 3. PDFs calculated over total intensities and Th_1 for different values of r below and above laser threshold. Panels (a) and (b) below laser threshold $\mu = 5$ respectively for $r = 1$ and $r = 2.4$. Panels (c) and (d) above laser threshold $\mu = 5.35$ respectively for $r = 1$ and $r = 2.4$.

It is seen from (a) that, for a fixed r, the system develops coexistent solutions associated to nonlasing, stationary CSs, chaotic CSs, and an extended turbulent state for certain values of the control parameter μ. While the entire branches of localized solutions appear below the laser threshold ($\mu_{th} = 5.18$), that of the extended turbulence still exists above the laser threshold. The coexistent solutions are also shown in (b) for fixed μ and varying r, which controls the slowness or fastness of the absorber material. Note that for the chosen values in (b) self-pulsing CSs appear as a new solution replacing stationary CSs for sufficiently high values of r.

III. TURBULENT STATE AND ROGUE WAVES

As already shown for this system of two dimensions in [7], the turbulent solutions contain spatiotemporal maxima which satisfy a variety of criteria defined for rogue waves. According to the widely accepted threshold for rogue waves in nonlinear optics, i.e., average of spatiotemporal intensities (or intensity maxima) plus eight times the standard deviations, the presence of rogue waves in these turbulence states is evident and their statistics has already been analyzed in [7]. For example, the probability density functions (PDFs) of total intensity and their deviation from certain statistics considering the RW threshold condition $Th_1 = \langle I \rangle + 8\sigma$, with σ being the standard deviation, are shown in Fig. 3 respectively below (a),(b) and above (c),(d) laser threshold. For this RW threshold, the deviation from a negative exponential function

$$\frac{\exp(-I/\langle I \rangle)}{\langle I \rangle} \tag{3}$$

is to be regarded as a signature of extreme events in the system.

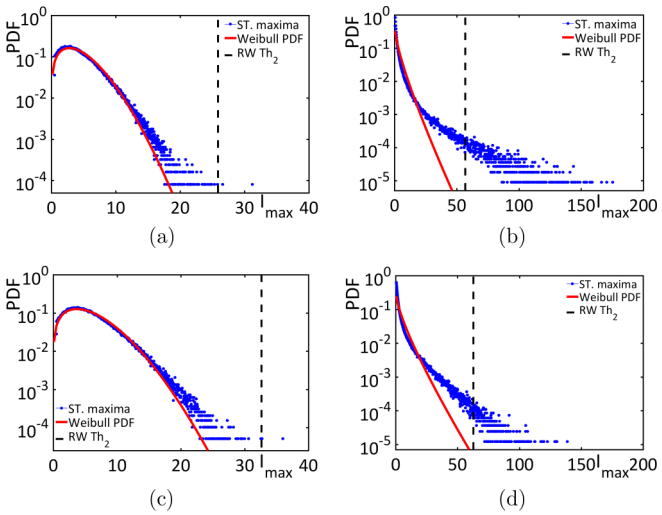

FIG. 4. PDFs calculated over spatiotemporal intensity maxima and Th_2 for different values of r below and above laser threshold. Panels (a) and (b) below laser threshold $\mu = 5$ respectively for $r = 1$ and $r = 2.4$. Panels (c) and (d) above laser threshold $\mu = 5.35$ respectively for $r = 1$ and $r = 2.4$.

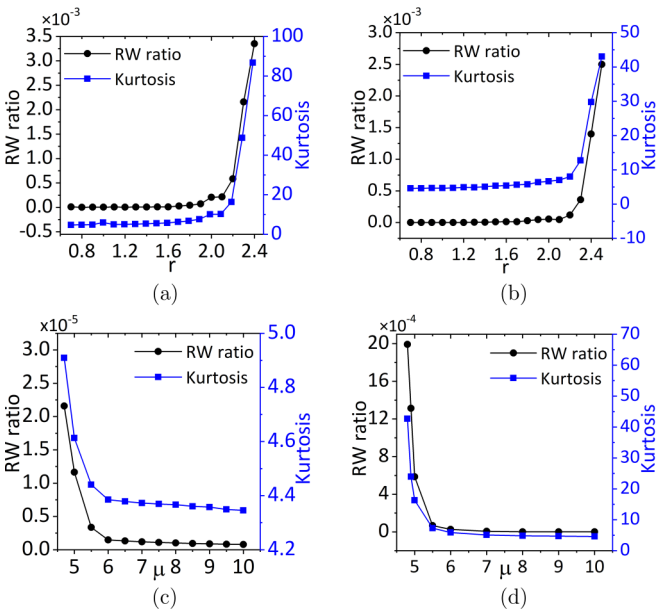

FIG. 5. Kurtosis and rogue wave ratio for (a) below $\mu = 5.0$ and (b) above $\mu = 5.35$ laser threshold with varying r. The same two parameters for varying μ and fixed r at (c) unity and (d) $r = 2.2$.

However, another definition for RWs has recently been introduced when considering the PDF of spatiotemporal maxima [7], as shown in Fig. 4 for the two cases of below (a),(b) and above (c),(d) the laser threshold. In this case, RWs are the spatiotemporal maxima lying above Th_2 defined as $Th_2 = \langle I_{\max} \rangle + 8\sigma$. In this case, the Weibull distribution

$$\frac{a}{b}\left(\frac{I_{\max}}{b}\right)^{a-1} \exp\left[-\left(\frac{I_{\max}}{b}\right)^{a}\right] \tag{4}$$

is a better choice to evidence the deviations leading to characterizing a wave as rogue wave. We stress that the PDF distributions shown here are not normal but still we can use averages and standard deviations to characterize them, which is not straightforward. These PDFs are shown in Fig. 4 for the two cases of below and above laser threshold.

There are also two other indicators which can be used besides the PDFs to observe the rogueness of the data: the kurtosis

$$\kappa = \frac{\frac{1}{n}\sum_{i=1}^{n}(I_i - \langle I \rangle)^4}{\left[\frac{1}{n}\sum_{i=1}^{n}(I_i - \langle I \rangle)^2\right]^2}, \tag{5}$$

which is the ratio of the fourth moment about the mean to the square of the variance, and the rogue wave ratio defined as the number of spatiotemporal events with intensities exceeding the intensity threshold Th_2 to the total number of spatiotemporal events during simulation. These are two useful guides in the parameter space when working with μ and r as the control parameters. Figures 5(a) and 5(b) show the variations in κ and RW ratio respectively for fixed pump current below and above laser threshold $\mu = 5.0, 5.35$ for varying r. These two parameters are also illustrated in Figs. 5(c) and 5(d) when r is respectively taken fixed at $r = 1, 2.4$ and μ is varying from below to above laser threshold. We can draw the conclusion from Fig. 5 that for lower pump and larger r values RWs are more probable to occur, which confirms the trends shown in [7]. By comparing Fig. 5 to Fig. 2 it seems that the presence of coexistent branches of extended turbulence, nonlasing, and localized solutions in lower pump values enhances the formation of RWs. On the other hand, the correlation between larger r values and larger kurtosis and RW ratio implies the fact that a faster absorber favors the formation of RWs.

Obtaining the frequency components of the chaotic intensity oscillations in the turbulent state can be useful in finding a probable correlation between the properties of RWs and the power of the involved frequencies. For this purpose, we have taken the Fourier spectrum of the output oscillations at the point in the transverse plane where the intensity is maximum, at an arbitrary point in the transverse plane and of the average intensity of the transverse plane. Figure 6 shows that, apart from its amplitude, the dominant frequency is the same and is roughly equal to ∼1.7 GHz in all three cases for the specific parameter values employed. Therefore, one should not be concerned with the type of intensity data collected (of an individual point or transverse average) when working with the power spectra and frequencies of such states of turbulence. We should also mention that the dominant frequency observed for the turbulent state is actually equal to the undamped relaxation oscillation frequency typical of semiconductor lasers which scales as $(\tau_p \tau_{\text{amp}})^{-1/2}$, where τ_p and τ_{amp} denote, respectively, the photon lifetime in the cavity and carrier lifetime in the amplifier material. This is a common feature in any free running class-B laser where $\tau_p \ll \tau_{\text{amp}}$ [42]. Here we are dealing with a semiconductor laser with saturable absorber that is different from a free running laser. We mention the relaxation oscillations here because we estimate that they are important to give an order of magnitude and we believe that still represents the typical frequency of the system.

The dominant frequency of intensity oscillations and its amplitude vary depending on the value of r which is shown

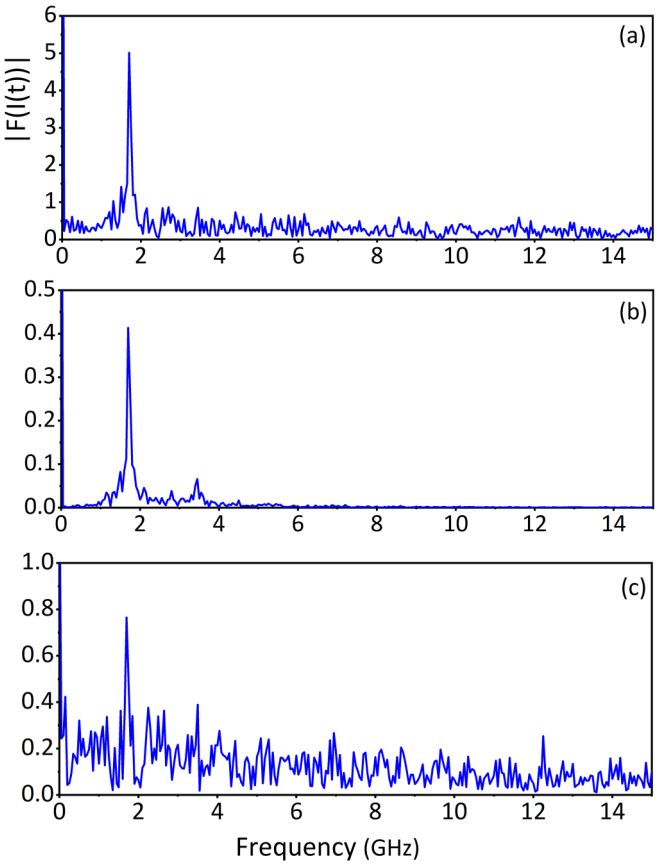

FIG. 6. Power spectra for the output intensity calculated (a) at the maximum intensity point in the transverse plane, (b) average intensity of the transverse plane, and (c) at an arbitrary point on the transverse plane. Parameter values are $\mu = 5$ and $r = 2.2$.

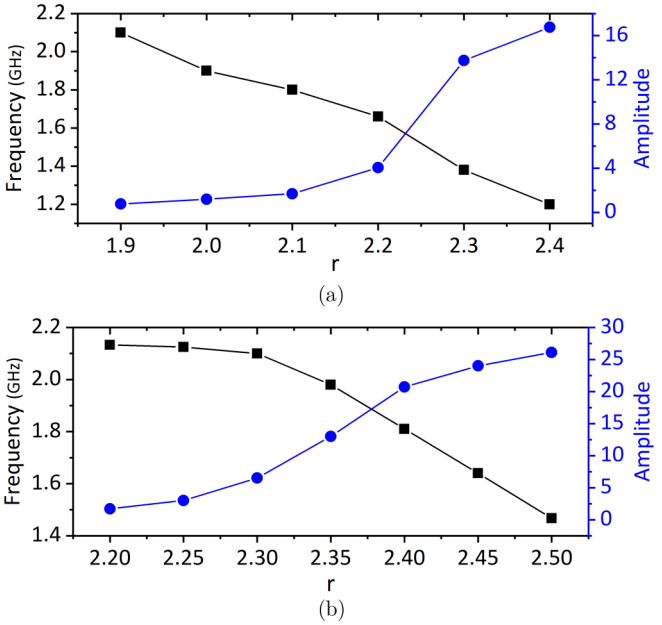

FIG. 7. Variations of the dominant frequency and its power (amplitude) in the turbulent branch (a) below laser threshold $\mu = 5$ and (b) above laser threshold $\mu = 5.35$.

in Fig. 7 for both below and above laser threshold. We observe that, regardless of the pump value μ, as r increases the dominant frequency of oscillations gradually decreases, while its power tends to increase. This is consistent with the fact that r is directly proportional to τ_{amp} through $r = \tau_{\text{amp}}/\tau_{abs}$ (τ_{abs} being the carrier lifetime in the absorber material), which appears in the denominator of the equation for the relaxation oscillation frequency. Also, when Fig. 7 is compared to Fig. 5, one realizes that increasing amplitude of the dominant frequency with r provides a more turbulent state with larger RW ratio and kurtosis, while the decreasing trend of the dominant frequency can be attributed to the slower rate of recombination in the active material as r increases.

IV. PARAMETER MODULATION AND ROGUE WAVES

In this section we turn our attention to the effect of parameter modulation, namely pump current, on the statistics and behavior of RWs. In this regard, we use the equation below which replaces μ in Eq. (1) for harmonic modulation of the pump parameter:

$$\mu(t) = \mu_0[1 + m\ \sin(2\pi f t)], \tag{6}$$

where m is the modulation strength and f is its frequency. In Fig. 8 the variations of the two indicators introduced in Sec. III for rogue waves, i.e., kurtosis and RW ratio, are shown for two different values of r in response to pump modulation. It is seen that when the modulation frequency coincides with the dominant frequency of oscillations, both indicators increase in value compared to their original values, which shows the resonant excitation feature typical of semiconductor gain media. It is also observed that in certain modulation frequencies the two indicators drop from their original values manifesting an off-resonance suppression. Enhancement and suppression of RWs indicated by RW ratio as a result of resonant or off-resonant modulations lie in the fact that the optical gain accumulation as the generating source of these giant waves is either fortified or repressed. This fact is shown in Fig. 9 where we show the extent of subspace made up of intensity and optical gain $(D + d - 1)$ in response to resonant and off-resonant modulations in the case of $r = 2.2$ illustrated in Figs. 8(a)–8(c). For the kurtosis, as a measure of the "tailedness" of the probability distribution, we observe that it is less affected by the off-resonant modulation in larger values of r since the state becomes more turbulent and the system is naturally more tailed. This is the opposite for resonant modulation since more RWs can be triggered contributing in even larger tailedness of the probability distribution.

It is interesting to check the capability of the proposed modulation-aided control of RWs to completely remove them and/or make them more often when the ratio of extreme events to the total number of events supported by the system is only marginal. For this purpose, we find a control parameter value for which the basins of attraction give the system its turbulent feature are located further away from those attractors which are responsible for giant excursions on the part of the trajectories. For example, for $r = 1.6$ RWs can only form in few numbers and it seems possible to fully suppress them. In Fig. 10, we show the power spectrum of the intensity oscillations for $r = 1.6$ and the corresponding

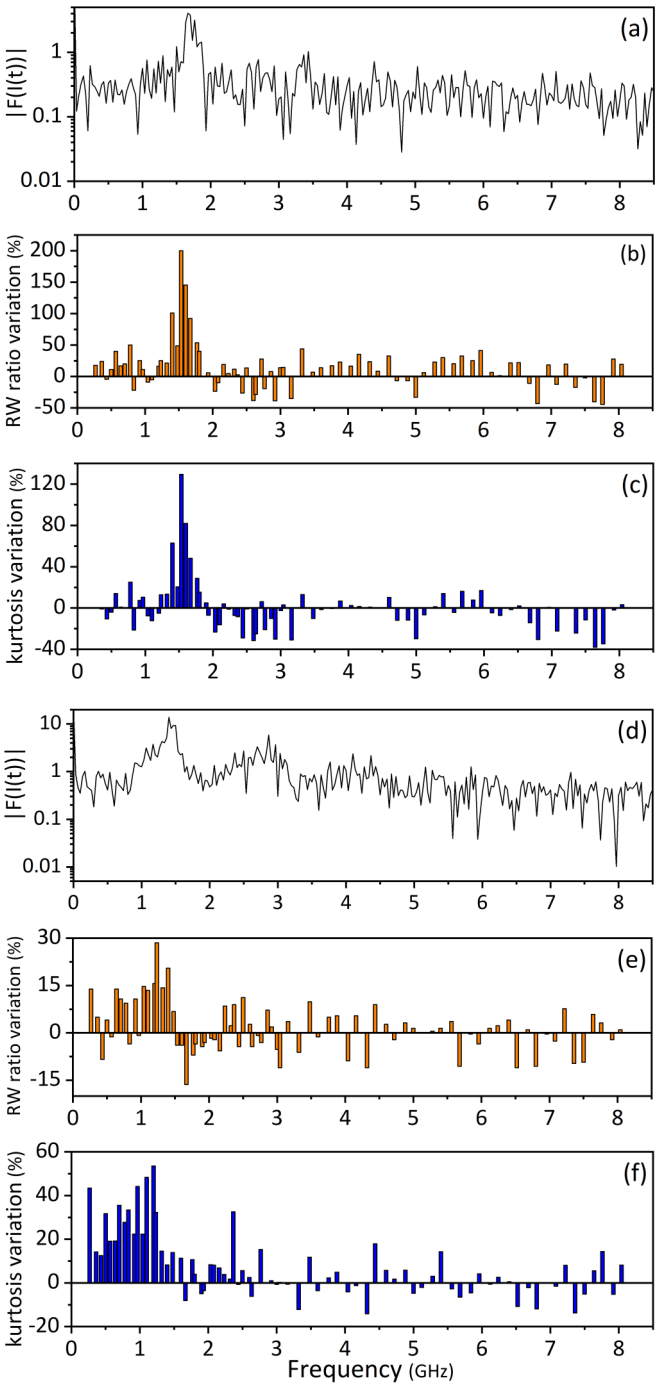

FIG. 8. Modulation response as RW ratio (b), (e) and kurtosis (c), (f) variations in percentage. For a better comparison, Fourier spectrum of the corresponding intensity oscillations is shown in (a), (d) in log scale. r is 2.2 for (a), (b), (c) and it is 2.3 for (d), (e), (f). Parameter values are $\mu_0 = 5$ and modulation amplitude $m = 0.015$.

RW ratio variation under the effect of harmonic modulations with different frequencies. The frequencies at which the RW ratio deviates maximally from that of the original are observed at 2.033 and 3.16 GHz, respectively, for enhancement and suppression. The result of modulation at these frequencies in comparison with the original situation in terms of spatiotemporal PDFs is shown in Fig. 11, which clearly supports the

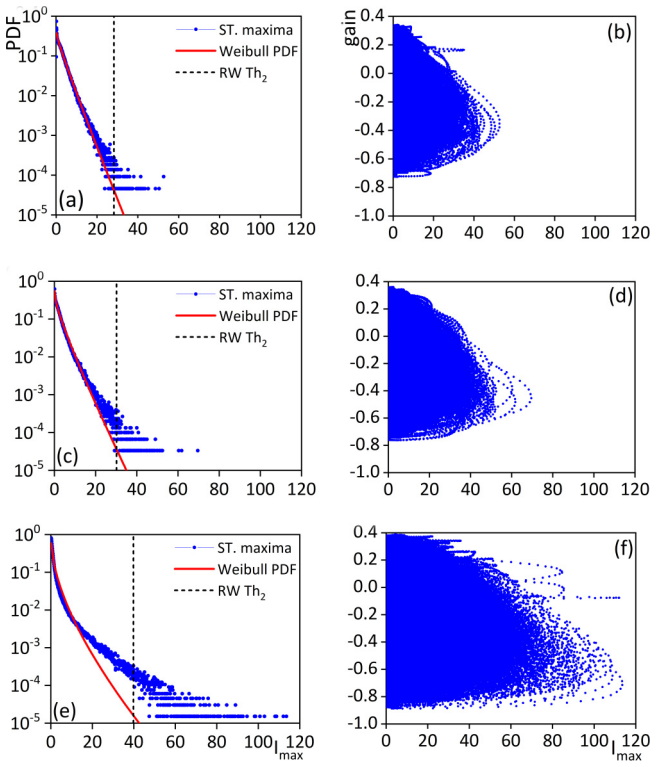

FIG. 9. PDFs of spatiotemporal maxima in off-resonant modulation with frequency 7.76 GHz (a), no modulation (c), and resonant modulation with frequency 1.53 GHz (e) along with their intensity-gain subspaces (b), (d), and (f), respectively. Parameter values are $\mu_0 = 5$, $r = 2.2$ and modulation amplitude $m = 0.015$.

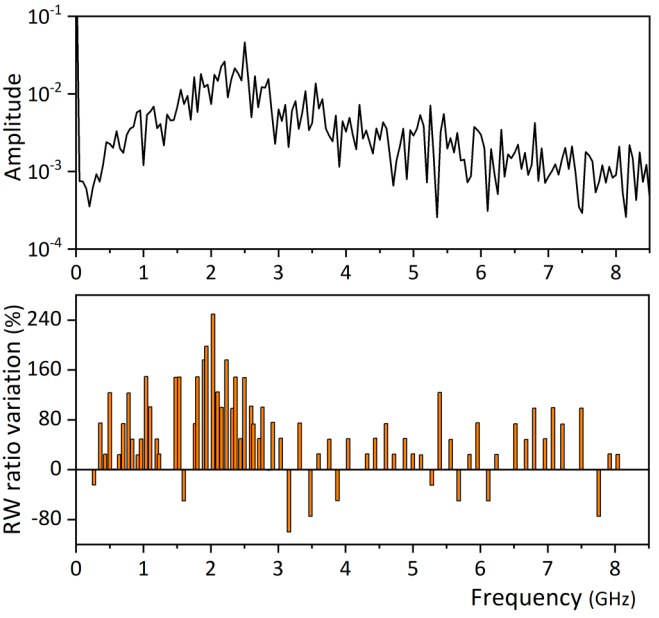

FIG. 10. Power spectrum of the intensity oscillations in the turbulent state and the corresponding deviations from the original RW ratio when modulated at different frequencies. Parameter values are $\mu_0 = 5$, $r = 1.6$ and modulation amplitude $m = 0.015$.

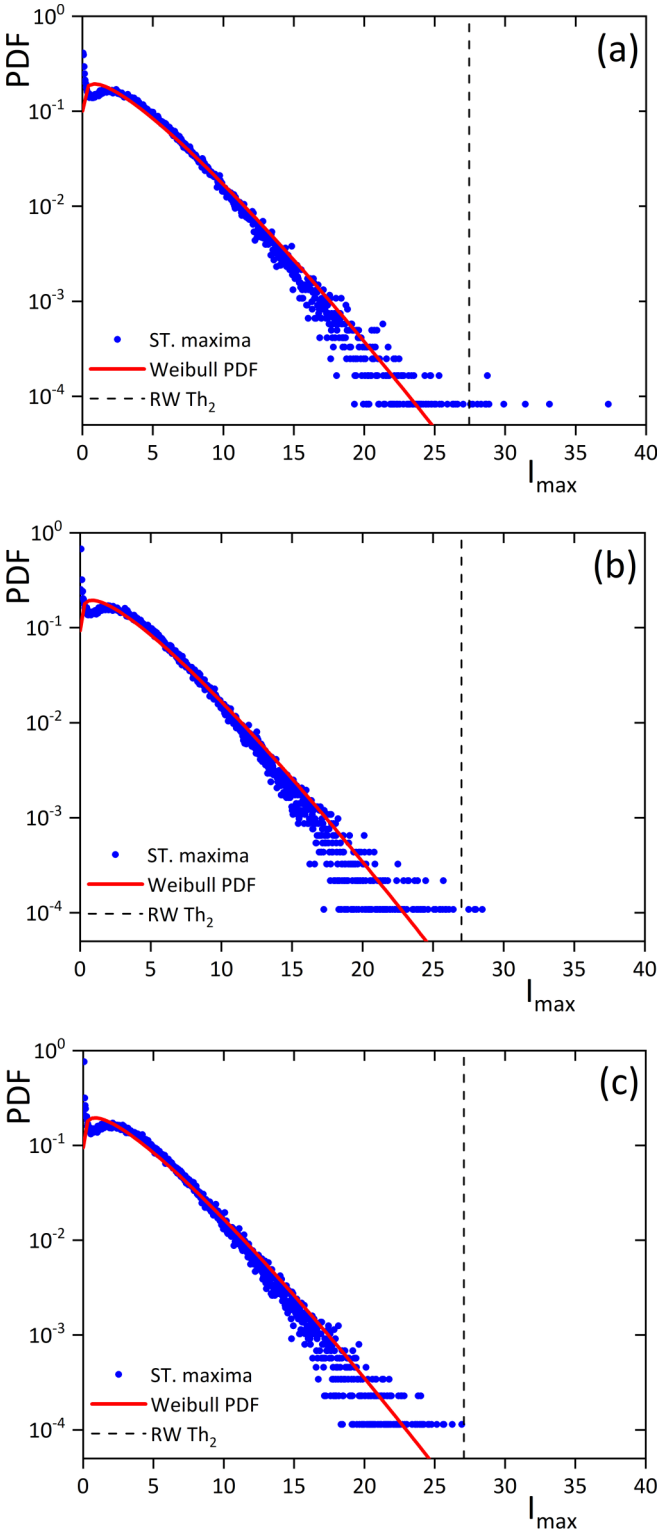

FIG. 11. Spatiotemporal maxima PDF when the system is (a) modulated resonantly at 2.033 GHz, (b) in its natural state, and (c) modulated off resonance at 3.16 GHz. Remarkable enhancement and full suppression at these special frequencies are evident which are consistent with data shown in Fig. 10. The values are $\mu = 5$, $r = 1.6$, and $m = 0.015$.

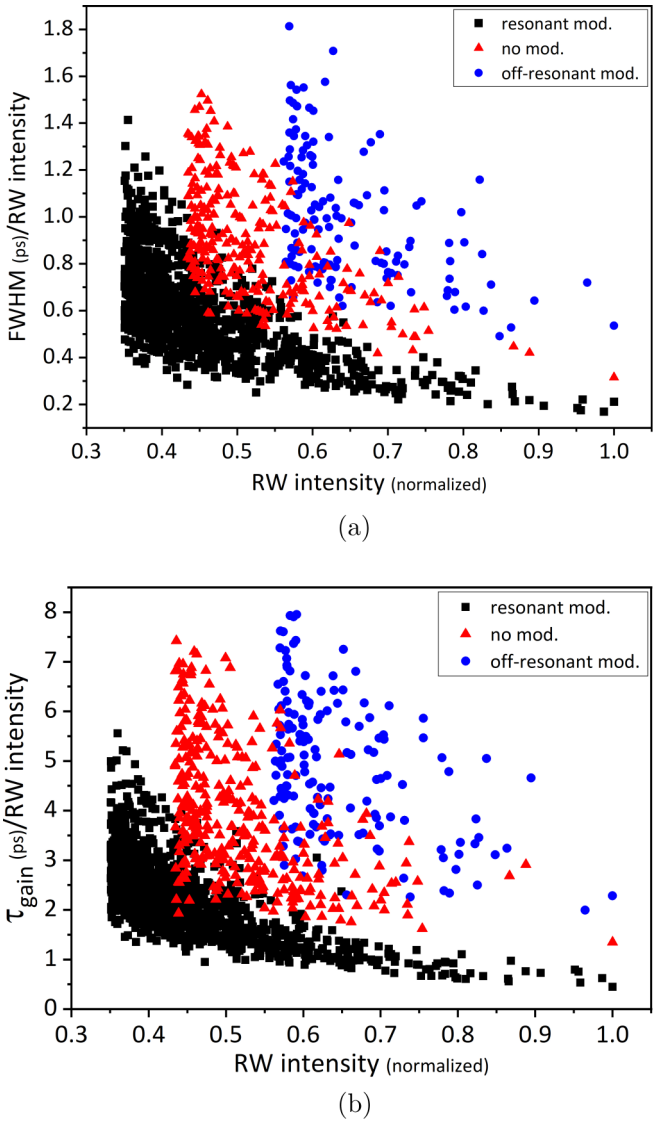

FIG. 12. Ratio of the intensity FWHM (a) and temporal width of the optical gain (b) to the corresponding RW intensity versus the RW intensities normalized to unity. We recall that all the data points shown in the figures are for RWs with intensities exceeding RW Th_2. The values are $\mu = 5$, $r = 2.2$, and $f = 1.53$, 7.76 GHz for resonant and off-resonant modulations, respectively.

idea of full suppression and enhancement when the RWs are only found scarcely. It is then concluded that one can employ the proposed control technique for various control parameter values either to generate RWs when the system normally does not support any or to fully remove RWs when the system generates plenty of them.

For the final remark, we note that modulation also affects other characteristics of the RWs such as their time duration. Similar to the previous discussions on the intensity values and statistics of the RWs, the effect on their time duration is more notable when the employed frequency is appropriately chosen for enhancement or suppression. As an example, we have

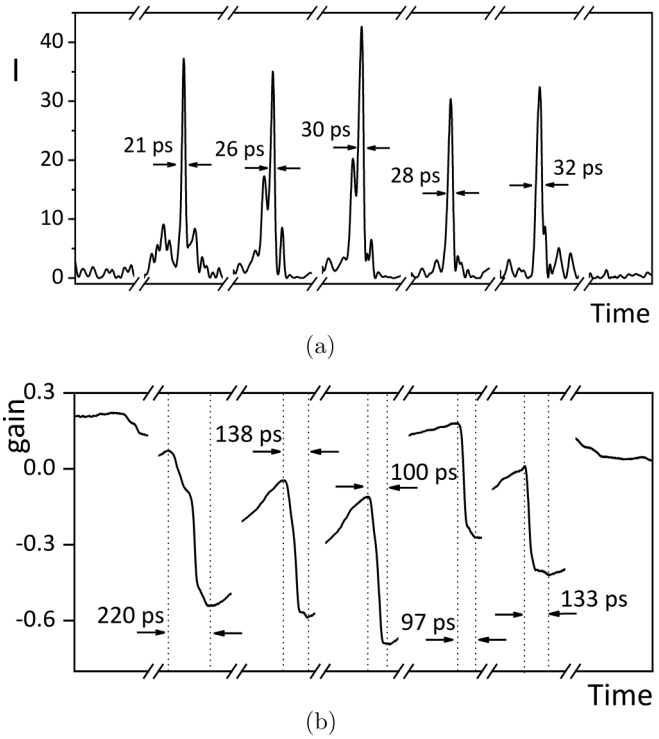

FIG. 13. Temporal width of intensity maxima (a) and optical gain dip (b) in a time window of 100 ns when no modulation is applied. Note that for the cases where two peaks form in a very close distance, intensity FWHM and temporal width of the optical gain dip are naturally broader which cannot be a counterargument for the presented discussions. The values are $\mu = 5$ and $r = 2.2$.

compared full width at half maximum (FWHM) of the RW intensities in terms of picoseconds in three cases of resonant, off-resonant, and no modulation. Figure 12(a) depicts the ratio of the FWHM of the RW intensity in picoseconds to the peak intensity of the corresponding RW versus the RW intensities which are normalized to unity. The same is done for optical gain in Fig. 12(b), where the ratio of the temporal width of the optical gain dip in picoseconds to the peak intensity of the corresponding RW is considered instead. We note that by gain dip temporal width we mean the time that it takes for the optical gain to drop from its maximum to its minimum at the time of RW formation. From Fig. 12(a), it is seen that as a result of resonant modulation RWs are born and die faster and this is the opposite for RWs under off-resonant modulation. It is also understood that higher intensity RWs have shorter lifetimes and that the lifetimes in the no-modulation case stand between those with resonant and off-resonant cases. These observations are supported by Fig. 12(b), where optical gain is considered. A typical time trace of intensity maxima and optical gain in an arbitrary point in the transverse plane are shown in Fig. 13 for a time window of 100 ns, which further supports the lifetime and optical gain dip arguments.

V. CONCLUSIONS

An effective technique is proposed to control the onset of extreme events in a broad-area semiconductor laser with saturable absorber. We showed by numerical experiments that modulation of a control parameter, here the pump current, can significantly enhance or suppress occurrences of rogue waves in the system. Supported by statistical analysis of the events and investigation of dynamical properties of intensity and optical gain, it is discussed that resonant modulations with frequencies close to that of the dominant oscillations in a turbulent state trigger more rogue waves with higher peaks and shorter duration compared to the case of no modulation. On the other hand, off-resonant modulations suppress rogue waves such that only those of larger intensity can survive now with smaller peaks but longer duration. This is in fact possible since resonant excitation favors the chaotic behavior by taking the state of the system closer to basins of attraction responsible for the large excursions in the trajectory. Off-resonant modulation instead restrains the formation of rogue waves by keeping the trajectory far from chaotic attractors. To further emphasize the feasibility of the proposed control technique to fully suppress the formation of RWs, in Fig. 11 we have deliberately chosen a control parameter value for which the RWs are only found in few numbers originally so that the full suppression can be realized through a small change of statistics. The applicability of the control scheme is guaranteed by many other simulations for a variety of control parameter values with much larger variations in the statistics, as shown in Figs. 8 and 9.

[1] D. R. Solli, C. Ropers, P. Koonath, and B. Jalali, Nature (London) **450**, 1054 (2007).
[2] N. Akhmediev, A. Ankiewicz, and J. M. Soto-Crespo, Phys. Rev. E **80**, 026601 (2009).
[3] B. Kibler, J. Fatome, C. Finot, G. Millot, F. Dias, G. Genty, N. Akhmediev, and J. M. Dudley, Nat. Phys. **6**, 790 (2010).
[4] D. J. Kedziora, A. Ankiewicz, and N. Akhmediev, Phys. Rev. E **88**, 013207 (2013).
[5] P. Suret, R. El Koussaifi, A. Tikan, C. Evain, A. Randoux, C. Szwaj, and S. Bielawski, Nat. Commun. **7**, 13136 (2016).
[6] C. Lecaplain, P. Grelu, J. M. Soto-Crespo, and N. Akhmediev, Phys. Rev. Lett. **108**, 233901 (2012).
[7] C. Rimoldi, S. Barland, F. Prati, and G. Tissoni, Phys. Rev. A **95**, 023841 (2017).
[8] S. Coulibaly, M. G. Clerc, F. Selmi, and S. Barbay, Phys. Rev. A **95**, 023816 (2017).
[9] C. Mayol, R. Toral, C. R. Mirasso, and M. A. Natiello, Phys. Rev. A **66**, 013808 (2002).
[10] D. Pierangeli, F. Di Mei, C. Conti, A. J. Agranat, and E. DelRe, Phys. Rev. Lett. **115**, 093901 (2015).
[11] D. Pierangeli, F. Di Mei, G. Di Domenico, A. J. Agranat, C. Conti, and E. DelRe, Phys. Rev. Lett. **117**, 183902 (2016).
[12] A. Mussot, A. Kudlinski, M. Kolobov, E. Louvergneaux, M. Douay, and M. Taki, Opt. Express **17**, 17010 (2009).

[13] J. M. Dudley, G. Genty, F. Dias, B. Kibler, and N. Akhmediev, Opt. Express **17**, 21497 (2009).
[14] C. Bonatto, M. Feyereisen, S. Barland, M. Giudici, C. Masoller, J. R. R. Leite, and J. R. Tredicce, Phys. Rev. Lett. **107**, 053901 (2011).
[15] J. Zamora-Munt, B. Garbin, S. Barland, M. Giudici, J. R. R. Leite, C. Masoller, and J. R. Tredicce, Phys. Rev. A **87**, 035802 (2013).
[16] F. Gustave, L. Columbo, G. Tissoni, M. Brambilla, F. Prati, B. Kelleher, B. Tykalewicz, and S. Barland, Phys. Rev. Lett. **115**, 043902 (2015).
[17] F. Gustave, L. Columbo, G. Tissoni, M. Brambilla, F. Prati, and S. Barland, Phys. Rev. A **93**, 063824 (2016).
[18] F. Gustave, C. Rimoldi, P. Walczak, L. Columbo, M. Brambilla, F. Prati, G. Tissoni, and S. Barland, Eur. Phys. J. D **71**, 154 (2017).
[19] C. Rimoldi, F. Gustave, L. Columbo, M. Brambilla, S. Barland, F. Prati, and G. Tissoni, Opt. Express **25**, 22017 (2017).
[20] P. Walczak, C. Rimoldi, F. Gustave, L. Columbo, M. Brambilla, F. Prati, G. Tissoni, and S. Barland, Opt. Lett. **42**, 3000 (2017).
[21] M. Eslami, M. Khanmohammadi, R. Kheradmand, and G.-L. Oppo, Phys. Rev. A **96**, 033836 (2017).
[22] G.-L. Oppo, A. Politi, G. L. Lippi, and F. T. Arecchi, Phys. Rev. A **34**, 4000 (1986); H. Solari and G.-L. Oppo, Opt. Commun. **111**, 173 (1994).
[23] *Extreme Events in Nature and Society*, edited by S. Albeverio, V. Jentsch, and H. Kantz (Springer, Berlin, 2005).
[24] N. Akhmediev, B. Kibler, F. Baronio *et al.*, J. Opt. **18**, 063001 (2016).
[25] J. Ahuja, D. B. Nalawade, J. Zamora-Munt, R. Vilaseca, and C. Masoller, Opt. Express **22**, 28377 (2014).
[26] S. Perrone, R. Vilaseca, J. Zamora-Munt, and C. Masoller, Phys. Rev. A **89**, 033804 (2014).
[27] D. Pierangeli, G. Musarra, F. Di Mei, G. Di Domenico, A. J. Agranat, C. Conti, and E. DelRe, Phys. Rev. A **94**, 063833 (2016).
[28] T. Jin, C. Siyu, and C. Masoller, Opt. Express **25**, 031326 (2017).
[29] M. Colet and A. Aragoneses, Sci. Rep. **8**, 10741 (2018).
[30] F. Selmi, S. Coulibaly, Z. Loghmari, I. Sagnes, G. Beaudoin, M. G. Clerc, and S. Barbay, Phys. Rev. Lett. **116**, 013901 (2016).
[31] M. Eslami, S. Z. Gandomani, F. Prati, H. Tajalli, and R. Kheradmand, J. Opt. **19**, 015502 (2017).
[32] M. Eslami, R. Kheradmand, and G.-L. Oppo, J. Phys. B: At., Mol., Opt. Phys. **53**, 075402 (2020).
[33] M. Bache, F. Prati, G. Tissoni, R. Kheradmand, L. Lugiato, I. Protsenko, and M. Brambilla, Appl. Phys. B **81**, 913 (2005).
[34] F. Prati, P. Caccia, G. Tissoni, L. A. Lugiato, K. Mahmoud Aghdami, and H. Tajalli, Appl. Phys. B **88**, 405 (2007).
[35] S. V. Fedorov, A. G. Vladimirov, G. V. Khodova, and N. N. Rosanov, Phys. Rev. E **61**, 5814 (2000).
[36] G.-L. Oppo, A. M. Yao, F. Prati, and G. J. de Valcárcel, Phys. Rev. A **79**, 033824 (2009).
[37] F. Prati, G. Tissoni, L. A. Lugiato, K. M. Aghdami, and M. Brambilla, Eur. Phys. J. D **59**, 73 (2010).
[38] M. Eslami, R. Kheradmand, and F. Prati, Phys. Rev. A **89**, 013818 (2014).
[39] M. Eslami, R. Kheradmand, P. Bahari, and H. Tajalli, Eur. Phys. J. D **69**, 222 (2015).
[40] M. Eslami, N. H. Khiavi, R. Kheradmand, and F. Prati, Phys. Rev. A **98**, 043807 (2018).
[41] H. Vahed, F. Prati, M. Turconi, S. Barland, and G. Tissoni, Philos. Trans. R. Soc. A **372**, 20140016 (2014).
[42] L. Lugiato, F. Prati, and M. Brambilla, *Nonlinear Optical Systems* (Cambridge University Press, Cambridge, UK, 2015).